Fast Single-Atom Preparation in Optical Tweezers via Rydberg Blockade

Yiyi Li,[1,*] Vernon M. Hughes,[1,2,*] Michael Peper,[1] Yicheng Bao,[1] Chenyuan Li,[1,2] Sanzhar Bissenali,[1,3] and Jeff D. Thompson[1,†]

[1]*Department of Electrical and Computer Engineering, Princeton University, Princeton, New Jersey 08544, USA*

[2]*Department of Physics, Princeton University, Princeton, New Jersey 08544, USA*

[3]*California Institute of Technology, Pasadena, California 91125, USA*

(Received 10 June 2026; accepted 21 September 2026; published 28 October 2026)

Continuously replenished optical tweezer arrays will unlock unlimited-depth quantum circuits with neutral atom qubits. A key bottleneck limiting the cycle time of these systems is removing atoms from tweezers initially loaded with more than one atom. In the conventional technique of light-assisted collisions, slow collisional dynamics limit the timescale for removing excess atoms to several milliseconds. Here, we propose and demonstrate a scheme for selectively removing one atom at a time from multiply occupied tweezers on a microsecond timescale, using intra-tweezer Rydberg blockade and autoionization. We demonstrate the protocol in ^{171}Yb in two complementary regimes. With two-photon Rydberg excitation from the ground state, we reduce the multi-atom probability to 1% in 64.8 μs, while retaining single atoms in 58.2(2)% of the tweezers, which is comparable to the filling fraction achieved with light-assisted collisions under the same experimental conditions, but over two orders of magnitude faster. With single-photon excitation from the metastable state $^3P_0$, reduced single-atom loss enables a higher filling fraction of 74.8(3)%, at the cost of additional temporal overhead to prepare the atoms in $^3P_0$. The final filling fraction is limited by an unexplained two-body loss mechanism, which, if solved, could enable fast, quasi-deterministic loading.

DOI: 10.1103/8t3p-x6s7

I. INTRODUCTION

Neutral atoms in optical tweezer arrays are a promising platform for fault-tolerant quantum computing [1–5], quantum simulation [6–11], and quantum metrology [12,13]. In all of these applications, quantum operations begin with a deterministically filled array of singly occupied optical tweezers. Preparing such arrays typically involves several stages, including atom loading from a magneto-optical trap (MOT), removal of multiply occupied tweezers via light-assisted collisions (LAC) [14,15], measuring the occupied sites, and atom rearrangement [16–18]. Historically, atom loading had the longest duration of all of these operations, which created little incentive to make the other steps faster. However, recent advances in fast atomic reloading from a cold reservoir have shortened atom loading times to the millisecond-scale [19–24], which makes the other steps rate-limiting.

There has been considerable progress on improving the speed of measurement through non-destructive measurements in free-space [25,26] and cavity arrays [27], as well as destructive measurements [28,29]. Similarly, many works have studied accelerated rearrangement protocols [30–32] and novel optical system architectures for fast rearrangement [33,34]. However, there has been less progress on improving the speed of single-atom preparation.

Loading atoms into an optical tweezer from a MOT or an atomic reservoir results in a Poisson distribution of atom occupancies. The prevailing approach to preparing singly occupied tweezers is light-assisted collisions [14,15], which eject atom pairs until the occupancy of each tweezer is either zero or one atom, reaching a steady-state filling fraction of 50%−60%. As LAC relies on molecular potentials acting over length scales of tens of nanometers, the resulting collisional rates of atoms in optical tweezers are small [35–37], leading to preparation times around 10 ms in typical optical tweezers, across many atomic species [20,23,24]. By tailoring the optical potentials used for LAC, the collision dynamics can be modified to preferentially remove one atom at a time,

*These authors contributed equally to this work.
†Contact author: jdthompson@princeton.edu

Published by the American Physical Society under the terms of the Creative Commons Attribution 4.0 International license. Further distribution of this work must maintain attribution to the author(s) and the published article's title, journal citation, and DOI.

increasing the final occupancy at the expense of increasing the preparation time to tens or hundreds of milliseconds [38–42]. We note that millisecond-scale LAC has been achieved in more tightly confining optical traps including 3D optical lattices [43] and nanofiber traps [44].

A conceptually distinct strategy exploits the Rydberg blockade for single atom preparation [45,46]. In this scheme, the Rydberg blockade is used to transfer at most one atom into a different hyperfine state, while the remaining atoms are pushed out of the trap. As the Rydberg interaction acts over micrometer length scales, the protocol duration is not limited by the rate of collisions between ground state atoms and is instead limited by the time required to eject atoms from the trap, which can be as short as 10 μs [1]. Using this *keep-one* approach, a single-atom preparation fidelity of 62% was achieved [46]. Extensions to higher single-atom occupancy with larger initial fillings have been proposed, but the practical performance is limited by collisions with nearby ground state atoms, Rydberg *spaghetti* effects, and long-range finite blockade effects [47–49].

In this work, we demonstrate a distinct method of using the Rydberg blockade to prepare singly occupied tweezers, using repeated cycles of Rydberg excitation and autoionization to eject extra atoms one at a time. This *remove-one* approach is fast—each cycle of Rydberg excitation and autoionization occurs on the microsecond timescale—and can reach high loading probabilities by avoiding multi-atom loss in a single cycle. In a ^{171}Yb tweezer array using two-photon Rydberg excitation from the ground state, we achieve 1% multi-atom occupancy with 18 cycles of excitation and ejection with a total duration of 64.8 μs, over two orders of magnitude faster than LAC under the same experimental conditions. The single-atom filling fraction is 58.2(2)%, which is limited by single-atom loss (2% per cycle) caused by ground-Rydberg decoherence from intermediate state scattering and finite Rydberg lifetime during the Rydberg excitation step. To circumvent this limitation, we apply the same approach using single-photon excitation to a Rydberg state with higher principal quantum number from the metastable state $^3P_0$. This reduces the single-atom loss to 0.26% per cycle and increases the final single-atom filling fraction to 74.8(3)%. However, in this regime, the single-atom occupancy becomes limited by an unexplained two-atom loss process, and the protocol duration extends to several milliseconds, because of the need to pre-cool atoms before transferring to $^3P_0$. This technique requires no additional hardware or control beyond what is already needed for high-fidelity two-qubit gates and can be implemented in any atomic species where fast Rydberg state removal can be engineered. Future work reducing the unexplained two-atom loss could enable fast, near-deterministic tweezer loading.

II. SINGLE-ATOM PREPARATION USING THE RYDBERG BLOCKADE

The basic mechanism underlying our protocol is illustrated in Fig. 1. For N atoms in a tweezer within the Rydberg blockade radius [Fig. 1(a)], the Rabi frequency of collective excitation to the singly excited state $|W\rangle = \frac{1}{\sqrt{N}}\sum_{i=1}^{N}|g_1\cdots r_i\cdots g_N\rangle$ is $\sqrt{N}\Omega$, where Ω is the single-atom Rabi frequency [50]. Applying a pulse with duration $T = 2\pi/\Omega$ returns the atom to the ground state when $N = 1$, but leaves one atom in the Rydberg state with probability $P(|W\rangle) = \frac{1}{2}(1-\cos(2\pi\sqrt{N}))$ when $N > 1$. Using autoionization to eject any Rydberg population at the end of the pulse from the trap [51–53], we can implement $N \to N-1$ population transfer, while preserving $N = 1$ population [Fig. 1(b)]. The process can be repeated until the multi-atom occupancy probability is reduced below the desired threshold P_{th}. An on-resonance 2π pulse also returns all atoms to the ground state when $\sqrt{N}$ is an integer ($N = 4, 9, \ldots$), which would lead to population accumulation at these atom numbers. This problem can be circumvented by detuning the Rydberg excitation by Δ, changing the Rabi frequency scaling to $\sqrt{N\Omega^2+\Delta^2}$.

A. Experimental setup

Using an apparatus previously described in Ref. [23], we first demonstrate the proposed scheme by performing Rydberg excitation from the ground state. In brief,

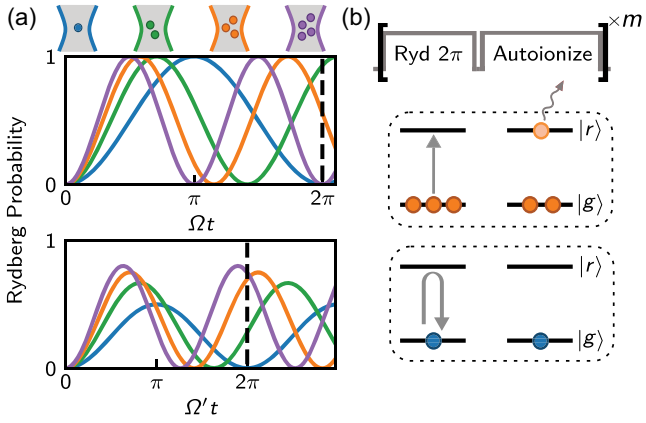


FIG. 1. (a) Collective Rabi oscillations for various atom numbers N (colors indicated in the legend), with on-resonance excitation (top) and detuned excitation (bottom, $\Delta = \Omega$ where the effective Rabi frequency is $\Omega' = \sqrt{\Omega^2+\Delta^2}$). Dashed lines denote single-atom 2π pulse durations. (b) Scheme for single-atom preparation, involving m cycles with two steps per cycle. First, a Rydberg 2π pulse excites one atom from a multiply occupied tweezer to the Rydberg state (orange), while keeping the atom in a singly occupied tweezer in the ground state (blue). Second, autoionization removes Rydberg population from the trap.

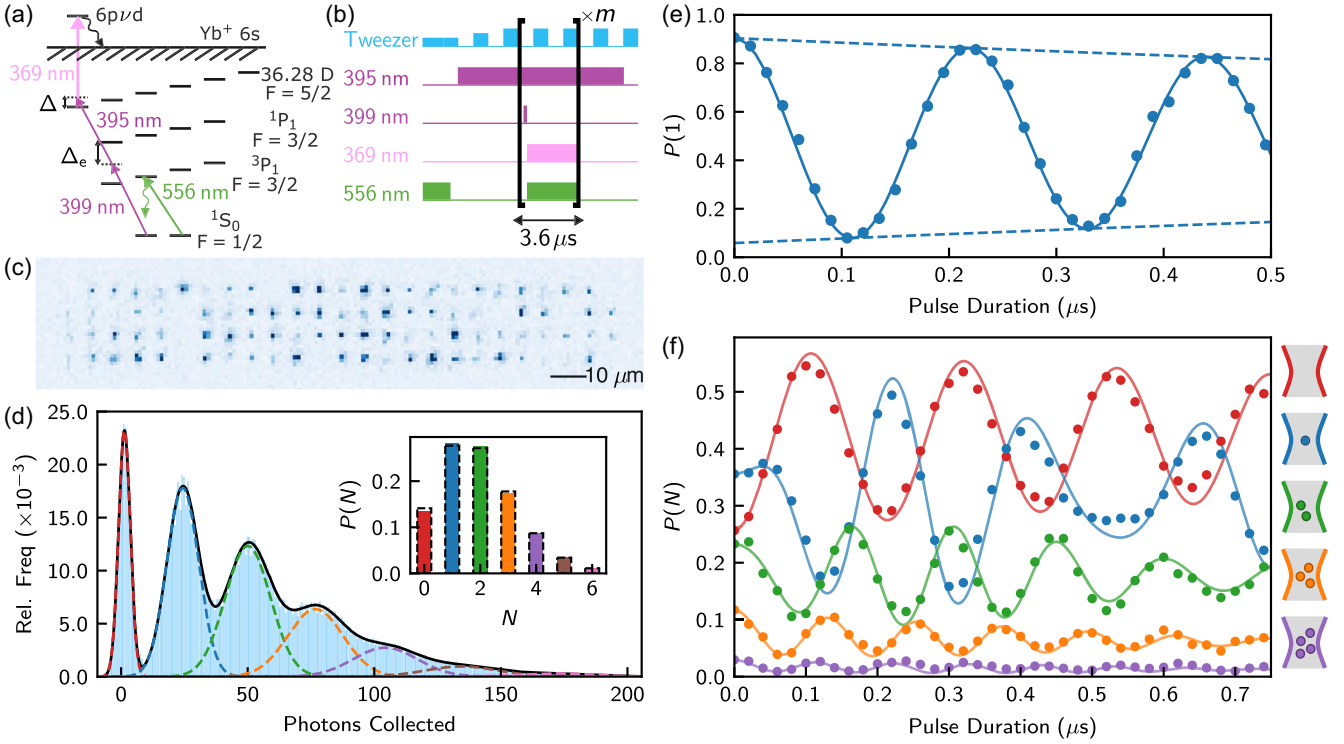


FIG. 2. (a) Relevant transitions for the two-photon excitation scheme. The 556 nm laser is used for optical pumping, 399 and 395 nm are used for two-photon Rydberg excitations, and 369 nm is used for autoionization of the Rydberg state. (b) Timing diagram of the protocol for the two-photon excitation scheme. (c) Exemplary single-shot image of the 4×25 tweezer array with number-resolved imaging. (d) Photon-count histogram of number-resolved images recorded after loading $\bar{N} = 1.9$ atoms per tweezer. Dashed lines show Gaussian fits for each atom number N, while the solid black line is the cumulative fit. The inset shows the extracted atom-number probability $P(N)$, compared with a Poisson distribution (black dashed bars). (e) Experimental data (circles) and simulation (solid line) of single-atom Rabi oscillations between the ground and Rydberg states, with a Rabi frequency of $\Omega/2\pi = 4.6$ MHz and detuning $\Delta = 0$. (f) Multi-atom collective Rabi oscillations. Circles show the measured probability $P(N)$ as a function of Rydberg pulse duration, for an initial average loading of $\bar{N} = 1.35$. Solid lines are simulation curves described in the main text. The Rabi frequency is $\Omega/2\pi = 4.7$ MHz, and the detuning is $\Delta/2\pi = -0.4$ MHz.

tweezers are loaded from a continuously maintained reservoir of cold ^{171}Yb atoms and subsequently transported out of the reservoir with a movable tweezer array. The atoms are then optically pumped into the $|g\rangle = |^1S_0, m_F = -1/2\rangle$ state using 556 nm light on the $^3P_1$ intercombination line [Fig. 2(a)], followed by excitation to the Rydberg state. The Rydberg state $|r\rangle = |36.28, L = 2, F = 5/2, m_F = -5/2\rangle$ is chosen such that the interaction strength V is large compared to the Rabi frequency for interatomic separations within a tweezer ($V/2\pi = 275$ MHz at $\sim$1 μm), but negligible for atoms in neighboring traps ($V/2\pi < 7$ kHz at 6.25 μm, see Appendix A). We use a two-photon excitation through an intermediate state $|e\rangle = |6s6p\,^1P_1\rangle$, with counterpropagating beams at wavelengths of 399 and 395 nm. Details of the laser parameters are given in Appendix B. To avoid anti-trapping of the Rydberg state and differential light shifts on the Rydberg transition caused by the tweezer light, we adiabatically ramp to intensity-modulated tweezers with a modulation period of 1.8 μs [4]. During the trap off period, we perform Rydberg excitation followed by an autoionization pulse with a 369 nm laser driving a transition to a $6p\nu d$ state. The Rydberg state is autoionized with a $1/e$ removal time of $\tau_{1/e} = 170$ ns. To ensure complete removal of Rydberg population, the autoionization pulse remains on until the next Rydberg excitation pulse, with a pulse duration of $\sim$3 μs. During the autoionization time, we also perform optical pumping again to transfer population that decayed to $|^1S_0, m_F = +1/2\rangle$ back to $|g\rangle$. To allow enough time for optical pumping, Rydberg excitation is performed during every other trap-off period. Each cycle consisting of a Rydberg 2π pulse, autoionization and optical pumping takes a combined 3.6 μs [Fig. 2(b)].

To characterize the protocol performance and probe collective Rydberg dynamics, we measure the atom occupancies in the optical tweezers by performing high-speed number-resolved imaging on the $^1S_0 \rightarrow {}^1P_1$ (399 nm) transition in 10 μs [26]. The imaging time is much shorter than the timescale of light-assisted collisions

by the imaging light, allowing the atom-number distribution in the tweezers to be measured before collisional loss occurs. An example single-shot image of the stochastically loaded 4×25 array is shown in Fig. 2(c), while a photon-count histogram is presented in Fig. 2(d). We extract the atom number distribution by fitting the photon-count histogram with a sum of seven Gaussian functions. The probability $P(N)$ is obtained from the enclosed area of each Gaussian function.

B. Collective intra-tweezer Rydberg dynamics

An example of single-atom Rabi oscillations is shown in Fig. 2(e), where the Rabi frequency is $\Omega/2\pi = 4.6$ MHz. The observed oscillations agree with a master-equation simulation using experimental parameters, and the visibility of the Rabi oscillations is limited by intermediate state scattering ($T_2^{\mathrm{Rabi}} = 2.7$ μs) and the Rydberg-state lifetime (7 μs).

To confirm that multiple atoms are blockaded within a tweezer, we measure the atom number distribution as a function of the Rydberg excitation duration [Fig. 2(f)]. The results exhibit complex multi-frequency Rabi oscillations, where the oscillation of $P(N)$ has components of $\sqrt{N}\Omega$ and $\sqrt{N+1}\Omega$. The complex multi-frequency oscillations are well captured by a master-equation-based simulation that incorporates the single-atom dynamics and Rydberg blockade, with an extra phenomenological dephasing rate Γ_N for atom numbers $N \geq 2$ (details of the simulation are discussed in Appendix B). This multi-atom decoherence is also observed in Refs. [46,47], where possible explanations include short-range effects from ground-Rydberg molecules or Rydberg *spaghetti* and long-range effects such as finite blockade [48,49,54].

C. Single-atom preparation performance

Now, we turn to demonstrating single-atom preparation using the approach. Figure 3(a) shows the probability to find zero, one or more than one atom in the tweezers after a variable number of repetitions, starting from $\bar{N} = 2.3$ atoms and using a detuning of $\Delta/\Omega = 0.75$. After $m = 18$ cycles (total duration 64.8 μs), the multi-atom probability reaches $P_{\mathrm{th}} = 1\%$ while maintaining a single-atom filling fraction of 58.2(2)%. For comparison, LAC using the same initial conditions and trap depth achieves a similar filling fraction at 1% multi-atom occupancy (53.9(2)%), but requires 10 ms [Fig. 3(b)]. Lowering the multi-atom threshold to 0.1% requires additional excitation cycles, increasing the protocol duration to 165.6 μs and reducing the final filling fraction to 35.6(4)%. This reduction in the filling fraction arises from single-atom loss, which is independently measured to be 2.0(2)% per cycle for the detuning $\Delta/\Omega = 0.75$, reduced from 5.4(1)% per cycle for on-resonant pulses due to decreased intermediate-state scattering and less time spent in the Rydberg state. This detuning is chosen to optimize the single-atom filling fraction at a target multi-atom occupancy of 1%, by balancing two competing

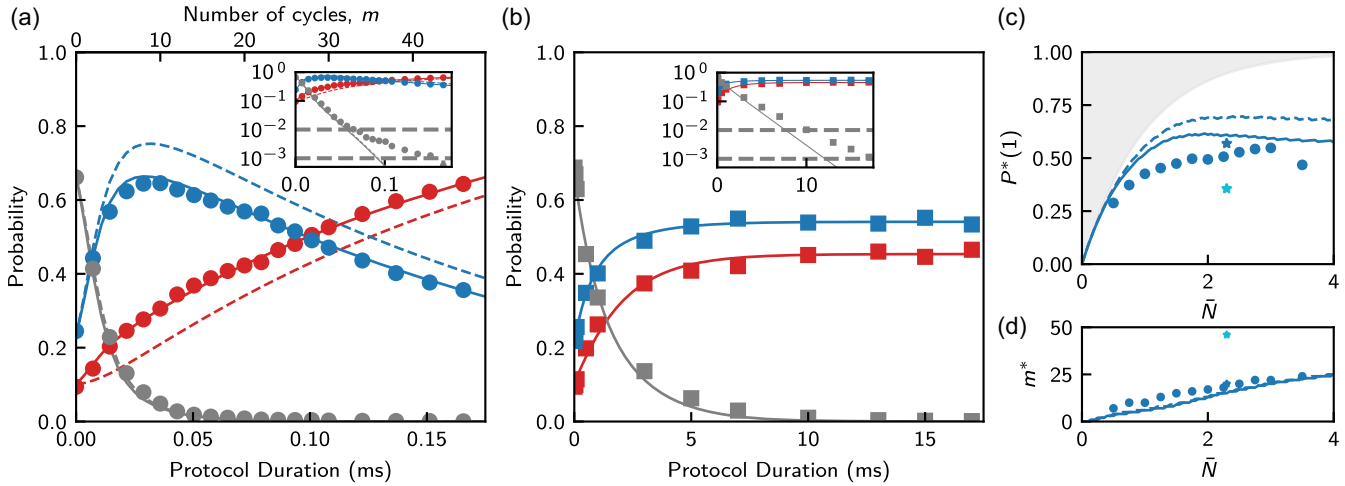


FIG. 3. (a) Experimental results (circles) and simulations (dashed and solid lines) for $P(0)$ (red), $P(1)$ (blue), and $P(>1)$ (gray) as a function of total protocol duration. Dashed lines depict master-equation-based simulations described in the main text. Solid lines include an additional 8% probability of $N = 2 \to 0$ loss per pulse. (b) Experimental data (squares) and simulations (solid lines) for LAC. The solid lines are based on population evolutions with fitted rates of $\gamma_{1\to0} = 0(3)$ s^{-1}, $\gamma_{2\to0} = 353(4)$ s^{-1}, and $\gamma_{2\to1} = 177(6)$ s^{-1}. The insets in (a,b) show the same data on a logarithmic y axis scale. The average initial number of atoms loaded is $\bar{N} = 2.3$ for both (a,b). (c) Single-atom filling fraction $P^*(1)$, after reaching $P(>1) < P_{\mathrm{th}}$, as a function of average number of atoms loaded, $\bar{N}$. The dark and light blue stars denote $P^*(1)$ for $P_{\mathrm{th}} = 1\%$ and 0.1%, respectively, extracted from the data in (a), while the circles depict the experimental results for $P_{\mathrm{th}} = 1\%$ from a different dataset. The dashed (solid) lines depict simulations without (with) the 8% probability of $N = 2 \to 0$ loss per pulse. The gray shaded region represents the initial $N = 0$ probability given by $e^{-\bar{N}}$. (d) The number of cycles required (m^*) to reach $P(>1) < P_{\mathrm{th}}$, as a function of average number of atoms loaded, $\bar{N}$.

effects: reducing single-atom loss during each cycle while limiting the number of cycles required to reduce the multi-atom population.

To understand the population evolution, we compare the measurements with master-equation simulations [dashed line in Fig. 3(a)]. However, we observe two effects not captured by the model. First, as shown in Fig. 3(a), the measured zero-atom population increases faster than predicted from single-atom loss alone, which can be empirically reproduced by including an 8% probability of $2 \to 0$ loss per cycle in the simulations [solid lines in Fig. 3(a)]. Second, we observe that the removal of multi-atom population slows down later in the protocol [inset, Fig. 3(a)], resulting in additional pulses compared to simulations for reaching lower multi-atom thresholds. Neither effect is understood.

The ultimate filling fraction, $P^*(1)$, is limited by the initial filling, single-atom losses, and two-atom losses. We study this systematically by varying the initial loading $\bar{N}$ by changing the tweezer loading time. As shown in Fig. 3(c), $P^*(1)$ initially increases with $\bar{N}$, reflecting the decreasing initial empty-tweezer probability $e^{-\bar{N}}$, but saturates near $\bar{N} = 2$. This trend is reproduced qualitatively by our simulations as above. We observe that the experimentally achieved filling fractions are systematically lower than the simulations, which we attribute to the simulations not capturing the observed slowdown described above. In addition, the discrepancy between the circle and star data arises from fluctuations in the 395 nm laser power, which changes the resonance and calibrated 2π pulse duration, leading to slightly higher single-atom loss for the circle data.

We find that prior cooling of the atoms in tweezers is not required for the protocol, avoiding additional temporal overhead. The atoms have a temperature of 80 μK, as set by the reservoir temperature. Cooling the atoms to 20 μK (requiring 1 ms) before the protocol does not significantly modify the observed dynamics, apart from additional LAC-induced losses during Doppler cooling. Additionally, no appreciable heating of the surviving atom is expected during the protocol, since the ejection mechanism through auto-ionization selectively removes the Rydberg atom while leaving the remaining ground-state atom unaffected. Although additional cooling is required for subsequent coherent qubit operations, this cooling can be incorporated into the identification imaging step performed after the protocol and therefore does not introduce additional temporal overhead.

III. SINGLE-ATOM PREPARATION WITH SINGLE-PHOTON RYDBERG EXCITATION

Further reducing the single-atom loss with two-photon excitation requires both suppressing intermediate-state scattering and choosing a Rydberg state with higher principal quantum number ν, which has a longer lifetime. Using the intermediate state $^1P_1$ in ytterbium, this is challenging because of both the difficulty of generating sufficiently high optical power at 395 nm and the broad linewidth of the $^1P_1$ state ($\Gamma/2\pi = 29.1$ MHz). This contrasts with alkali-atom platforms, where low-loss two-photon Rydberg excitation is readily achievable [55]. We overcome this limitation by using single-photon excitation from the metastable $^3P_0$ state [28].

To prepare atoms in $|^3P_0, m_F = +1/2\rangle$, we perform cooling (4 ms), followed by state preparation (2.5 ms), consisting of 1.9 ms for ramping the trap intensity and modulation, and 660 μs of optical pumping by driving a Raman transition to the $5d6s^3D_1$ state [28] [Fig. 4(a)]. Accidental light-assisted collisions during cooling lead to a sub-Poissonian atom-number distribution even without applying any Rydberg pulses, yet the majority of tweezers remain multiply occupied [Fig. 4(b)]. Atom occupancies are measured after the protocol by depumping the $|^3P_0, m_F = +1/2\rangle$ atoms back to the ground state. Additional details of the experimental implementation are given in Appendix C.

We excite to the Rydberg state $|r'\rangle = |\nu = 52.31, L = 0, F = 1/2, m_F = -1/2\rangle$, chosen for compatibility with high-fidelity two-qubit gates [56], from $|^3P_0, m_F = +1/2\rangle$ using a single-photon transition driven by a 302 nm laser. Representative single-atom Rabi oscillations and coherent multi-atom Rabi oscillations between $|^3P_0, m_F = +1/2\rangle$ and $|r'\rangle$ with a Rabi frequency of $\Omega/2\pi = 6$ MHz are shown in Figs. 4(c) and 4(d). The single-atom loss is reduced to 0.26(2)% per 2π pulse because of the absence of intermediate-state scattering and the longer lifetime of the higher-ν Rydberg state.

The reduced single-atom loss enables higher single-atom filling fractions than in the two-photon implementation. We achieve a filling fraction of 74.8(3)% when reaching a multi-atom probability below $P_{\text{th}} = 1\%$ in $m = 11$ cycles, and a filling fraction of 72.4(3)% when $P_{\text{th}} = 0.1\%$ with 24 cycles [Fig. 4(e)]. In contrast to the two-photon implementation, where extending the protocol to lower P_{th} leads to a significant reduction in $P^*(1)$, the single-photon implementation exhibits only a ∼2% decrease in filling fraction between these thresholds because of the low single-atom loss. The pulse repetition period was chosen to be 7.2 μs, resulting in a time of 79.2 μs to reach $P_{\text{th}} = 1\%$ and 172.8 μs to reach $P_{\text{th}} = 0.1\%$. This choice was made for experimental convenience and was not optimized. Since the protocol performance is primarily determined by the per-cycle removal dynamics, the longer repetition period does not reflect a fundamental limitation of the single-photon implementation. With this approach, filling fractions above 70% can be achieved with an average number of atoms as low as $\bar{N} = 1.5$ at $m = 0$ [Figs. 4(f) and 4(g)].

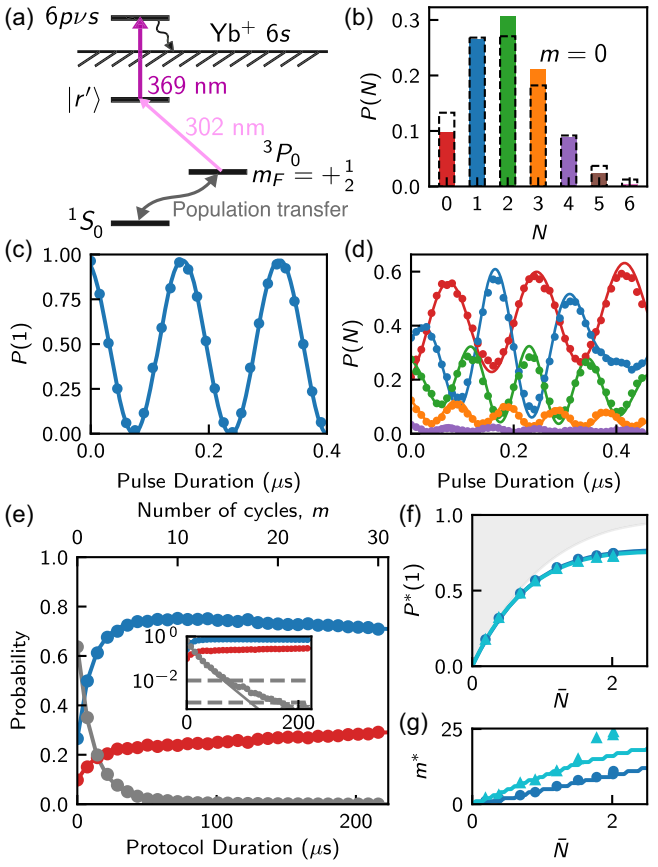


FIG. 4. Single-atom preparation with single-photon Rydberg transitions. (a) Relevant energy levels for single-photon transitions from the metastable $^3P_0$ state. (b) Probability distribution of atom number without applying Rydberg pulses (colored bars), compared with a Poisson distribution (black dashed bars). (c) Exemplary single-atom Rabi oscillations. (d) Multi-atom collective Rabi oscillations, measured with $\bar{N} = 1.4$. (e) $P(0)$ (red), $P(1)$ (blue), and $P(>1)$ (gray) as a function of the protocol duration, starting from $\bar{N} = 2.0$. The protocol duration here does not include cooling and $^3P_0$ state preparation overhead. The inset depicts logarithmic scaling of the y axis, with dashed lines showing $P_{\text{th}} = 10^{-2}$ and $P_{\text{th}} = 10^{-3}$ and solid lines showing the simulation results. (f) The single-atom filling fraction, $P^*(1)$, after reaching $P(>1) < P_{\text{th}}$ as a function of the average number of atoms $\bar{N}$ at $m = 0$ cycles. The gray shaded region represents the initial $N = 0$ probability. (g) The number of cycles required (m^*) to reach $P(>1) < P_{\text{th}}$. In panels (f,g), the dark blue circles denote experimental data with $P_{\text{th}} = 1\%$ and the light blue triangles correspond to $P_{\text{th}} = 0.1\%$. The solid lines in panels (d–g) are based on simulations as described in Appendix C.

The achieved single-atom filling fraction is no longer limited by single-atom loss, but instead by the observed $N \to N-2$ loss, which is evident in the sharp rise of $P(0)$ probability in the first few rounds of the protocol. The $N = 2 \to 0$ loss probability is fitted to be 18% per cycle, over 2× larger than the losses observed with the two-photon implementation. The origin of this two-body loss remains unclear. Possible mechanisms include blockade violations via *Rydberg spaghetti* [49] at short interatomic distances, or effects from Rydberg atoms interacting with nearby $^3P_0$ atoms in the form of molecules or collisions [48,54,57,58]. Loss induced by all of these processes is expected to increase as close atom pairs become more likely, and they are therefore expected to exhibit qualitatively similar dependence on density, atom number, and temperature. These dependences may not clearly distinguish the underlying mechanism. Potentially more informative signatures could arise from the dependence on the chosen Rydberg state. However, how the Rydberg spaghetti and molecular contributions depend on the Rydberg state is not known, and quantitative predictions are challenging because they require modeling short-range Rydberg interactions and molecular states. Future systematic studies could provide additional constraints by varying the principal quantum number or detuning. For example, spectroscopic features or resonances associated with molecular states could help determine whether molecular effects contribute to the observed two-body loss.

The total duration of the entire single-atom preparation sequence is 6.6 ms, where the time required for cooling and state-preparation of atoms in $^3P_0$ accounts for the majority of the total protocol duration. The fast timescale of the remove-one protocol therefore shifts the dominant preparation overhead to laser cooling and internal-state preparation, providing additional motivation for the development of faster cooling techniques [25,59].

IV. DISCUSSION

We have demonstrated a fast single-atom preparation protocol in optical tweezers, achieving over two orders of magnitude speedup compared to conventional light-assisted collisions by exploiting intra-tweezer Rydberg blockade. The essential ingredients for this protocol are low-loss Rydberg excitation and fast removal of Rydberg atoms. Low-loss Rydberg excitation can be readily achieved with tweezer-array experiments using the same ingredients necessary to achieve high-fidelity two-qubit gates. Autoionization is a generic feature of alkaline earth atoms [51,53] but can be replaced by other Rydberg removal techniques such as anti-trapping or field ionization [60–62].

This protocol can in principle be extended to deterministic loading, due to the $N \to N-1$ ejection mechanism and the high survival probability of single atoms. Operating in the near-deterministic regime could eliminate the need for taking a non-destructive image and rearrangement, removing the other two processes with major temporal overhead in operating a continuous tweezer array. Two-body losses are the main obstacle to achieving higher filling fractions; their origin is not yet understood, and they are observed to be 8% for our two-photon implementation from the ground state and 18% for our

single-photon implementation from the metastable state. A single-atom filling fraction of 99% can be reached with single and two-atom losses of 0.1% and 0.05%, respectively, starting from $\bar{N} = 6$ atoms per tweezer (see Appendix D). This initial loading is lower than our estimate of $\bar{N} \approx 60$ for reaching the same level of determinism with the *keep-one* approach [46].

ACKNOWLEDGMENTS

We acknowledge helpful conversations with Genyue Liu, Guillaume Bornet, Bichen Zhang, Deniz Kurdak, and Mingxuan Xiao. This work was supported by the Gordon and Betty Moore Foundation (Grant DOI 10.37807/gbmf12253), the Army Research Office (W911NF2410358), the National Science Foundation through the CAREER program (PHY-2047620), DARPA MeasQuIT (HR00112490363), the Office of Naval Research (N00014-23-1-2621), and the NSF Center for Robust Quantum Simulation (OMA-2120757). J. D. T. is a co-founder and shareholder of Logiqal, Inc.

DATA AVAILABILITY

There are no publicly available research data or software supporting this manuscript. Requests for further information or data should be sent to the authors.

APPENDIX A: CHOICE OF RYDBERG STATES

We choose the Rydberg states and tweezer spacings such that the interaction strengths are large for atoms within the same tweezer, ensuring strong blockade during Rydberg excitations, while remaining weak for atoms in neighboring tweezers. To estimate the relevant interaction scales under the experimental trapping conditions, we calculate distributions of effective Rydberg interaction strengths

$$V_{\mathrm{eff}}(R,\theta) = \left(\sum_k \left|\frac{c_k(R,\theta)}{\Delta_k(R,\theta)}\right|^2\right)^{-1/2}, \tag{A1}$$

where the interacting pair eigenstates, $|\Phi_k(R,\theta)\rangle$, are obtained by diagonalizing the interaction Hamiltonian in the basis of bare atomic pair states, $|r_i r_j\rangle$. The coefficient $c_k(R,\theta) = \langle\Phi_k(R,\theta)|rr\rangle$ gives the overlap of the target bare pair state $|rr\rangle$ with interacting eigenstate $|\Phi_k(R,\theta)\rangle$, while $\Delta_k(R,\theta)$ denotes the corresponding energy defect. We use the effective interaction strength, V_{eff}, as a practical estimator of the blockade against perturbative off-resonant double excitation. Here, θ is the angle between the internuclear axis and the quantization axis defined by the magnetic field. Based on the thermal atomic position distributions of R and θ, the resulting atom-pair-interaction-strength distributions for the two-photon and single-photon excitation schemes are shown in Fig. 5. The spread of the intra-tweezer distributions reflects

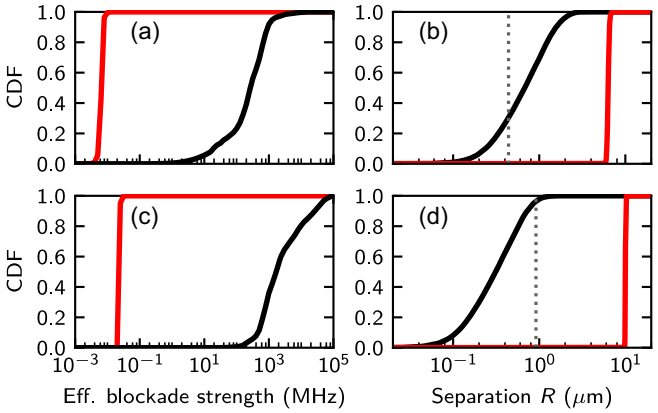


FIG. 5. Cumulative distribution functions (CDF) of (a,c) effective Rydberg interaction strengths and (b,d) interatomic separations R, for atom pairs within the same tweezer (black) and in neighboring tweezers (red): (a,b) for the $|36.28, L = 2, F = 5/2\rangle$ state, for a temperature of $T = 80$ μK and trap frequencies $(\omega_{\mathrm{rad}}, \omega_{\mathrm{ax}}) = 2\pi \times (89\ \mathrm{kHz}, 15\ \mathrm{kHz})$, with an inter-tweezer spacing of 6.25 μm and (c,d) for the $|52.31, L = 0, F = 1/2\rangle$ state for a temperature of $T = 9$ μK and trap frequencies $(\omega_{\mathrm{rad}}, \omega_{\mathrm{ax}}) = 2\pi \times (65\ \mathrm{kHz}, 11\ \mathrm{kHz})$, with an inter-tweezer spacing of 10 μm. In (b,d), the dotted vertical line marks the LeRoy radius, below which the multipole expansion underlying the interaction table used in (a,c) is expected to become unreliable.

contributions from both the thermal spread in R and the angular anisotropy of the interaction at short interatomic distances. Figure 5 shows the cumulative distribution of interatomic separation R, for both intra-tweezer and inter-tweezer pairs, for each Rydberg state. The mean intra-tweezer separations are $\bar{R} = 0.81$ μm for the $|36.28, L = 2\rangle$ scheme ($T = 80$ μK) and $\bar{R} = 0.37$ μm for the $|52.31, L = 0\rangle$ scheme ($T = 9$ μK), reflecting the different trap temperatures. For comparison, the LeRoy radius, $R_{\mathrm{LR}} = 4\sqrt{\langle r^2\rangle}$, which characterizes the distance scale around which the multipole expansion underlying our pair-interaction model begins to break down, is 0.44 and 0.96 μm for the two states, respectively. Consequently, approximately 30% of within-tweezer pairs for the $|36.28, L = 2\rangle$ scheme and 96% for the $|52.31, L = 0\rangle$ scheme lie at separations below the corresponding LeRoy radius.

APPENDIX B: DETAILS OF RYDBERG EXCITATION FROM THE GROUND STATE

1. Experimental details

To excite ground state atoms to the Rydberg state $|r\rangle$, we use a two-photon excitation with typical Rabi frequencies of $\Omega_{399}/2\pi = 130$ MHz (beam power $P = 2$ mW, beam waist $w_0 = 500$ μm) and $\Omega_{395}/2\pi = 70$ MHz ($P = 280$ mW, $w_0 = 50$ μm), and an intermediate state detuning of $\Delta_e/2\pi = -1020$ MHz. The sign $\Delta_e\Delta_r < 0$ is chosen to mitigate intermediate state

scattering [55]. After Rydberg excitation, an autoionization pulse drives a transition to a $6p\nu d$ state lying energetically above the Yb^+ ion core. Approximately 93% of the Rydberg population is ionized ($P_{369} = 18$ mW, $w_0 = 50$ μm, $\tau_{1/e} = 170$ ns), limited by the finite Rydberg lifetime and scattering of the $|r\rangle$ state back to $|g\rangle$ induced by 395 nm photons. The protocol is performed in 488 nm tweezers with depth of 380 μK. The magnetic field of 8.5 G is oriented perpendicular to the tweezer axial direction. Due to the orientation of the beams with respect to the 4×25 tweezer array, we only select out 50 traps lying along the direction of propagation of the beams for analysis of experiments involving Rydberg dynamics. To evaluate the protocol performance when multi-atom probabilities are less than a few percent, we employ thresholding rather than fitting $P(N)$ by Gaussian functions.

2. Simulation details

For the two-photon Rydberg excitations from $^1S_0$, we model the Rabi oscillations and protocol with master-equation-based simulations with collapse operators to account for intermediate state scattering and finite Rydberg lifetime. For multiple atoms within a tweezer, we account for the Rydberg blockade with a $V/2\pi =$ 100 MHz interaction energy for pairs of atoms in the Rydberg state.

Our measurements of the $^1S_0$ population also include Rydberg atoms that are not properly autoionized and return to the ground state via decay or scattering. We account for this in simulations by multiplying the Rydberg population at the end of the Rydberg pulse by a fixed probability of autoionizing a Rydberg atom. The autoionization probability is 93%, which was independently computed based on measurements of the autoionization timescale, Rydberg lifetime, and inferred 395 nm scattering. This probability is used for Figs. 2(e) and 3; however, we find a better fit to the data in Fig. 2(f) with an autoionization probability of 90%, likely as a result of fluctuating 369 nm laser intensity.

For multiple atoms within a tweezer, we include an extra dephasing collapse operator $\sqrt{\Gamma_N}\sigma_z$. We fit Γ_N for $N = 2$ through $N = 4$ to minimize the residuals between the simulated values and experimental data from Fig. 2(f). The fitted values are $\Gamma_2/2\pi = 0.116(3)$ MHz, $\Gamma_3/2\pi = 0.194(6)$ MHz, and $\Gamma_4/2\pi = 0.18(3)$ MHz.

APPENDIX C: DETAILS OF RYDBERG EXCITATION FROM THE $^3P_0$ STATE

1. Experimental details

In order to limit atom losses during the preparation and readout of $^3P_0$, it is necessary to cool the atoms using gray-molasses cooling detailed in Ref. [23]. The atomic temperature of the $^3P_0$ atoms when the protocol is performed is 9 μK. Light-assisted collisions during the cooling process result in a sub-Poissonian distribution of the atom number, as well as higher temperatures for multiple atoms in a trap due to collisional heating. The sub-Poissonian atom distribution after cooling, pumping to $^3P_0$, and depumping can be modeled by a Mandel parameter $Q = \frac{\sigma_N^2}{\bar{N}} - 1$ ranging from 0 to −0.25 for $\bar{N} = 0$ through $\bar{N} = 2.0$. For simulations in Figs. 4(f) and 4(g), we interpolate Q linearly in this range to approximate the initial atom distributions prior to Rydberg evolution.

After cooling, atoms are prepared in the metastable state $|^3P_0, m_F = +1/2\rangle$ using optical pumping. First, we apply a global σ^+ 556 nm beam that drives the $|^1S_0, m_F = -1/2\rangle \rightarrow |^3P_1, m_F = +1/2\rangle$ transition to prepare the atoms in $|^1S_0, m_F = +1/2\rangle$ state. Then, we coherently excite atoms to $5d6s^3D_1$ using a two-photon Raman transition $|^1S_0, m_F = 1/2\rangle \rightarrow |^3P_1, m_F = 3/2\rangle$ (556 nm) and $|^3P_1, m_F = 3/2\rangle \rightarrow |5d6s^3D_1, m_F = 3/2\rangle$ (1539 nm). The $5d6s^3D_1$ state decays into the desired $|^3P_0, m_F = +1/2\rangle$ state, as well as $6s6p^3P_1$ and $6s6p^3P_2$. $6s6p^3P_1$decays back to $^1S_0$ and is pumped again, and $6s6p^3P_2$ is constantly depumped through the $6s6d^3D_2$ state using a 497 nm laser. The $^3P_0$ atoms are trapped in 488 nm tweezers with trap depth of 220 μK. The magnetic field of 75 G is oriented perpendicular to the tweezer axial direction. To readout the atom population, we use the spin-selective depumping scheme detailed in Ref. [23] to only transfer atoms in $|^3P_0, m_F = +1/2\rangle$ back to $^1S_0$ prior to number-resolved imaging.

A 302 nm laser with σ^- polarization, power of $P =$ 73 mW and beam waist of $w_0 = 20$ μm is used to drive the $|^3P_0, m_F = +1/2\rangle$ to the Rydberg state $|r'\rangle$. Since this $|r'\rangle$ state has a higher ν compared to the state chosen for the ground state excitation, the interaction strength and blockade radius are larger, so we increase the tweezer spacing to 10 μm. As a result of this larger spacing and the smaller beam waist of the 302 nm laser, the protocol performance is characterized in a 1D array of 7 atoms. The autoionization removal time of the $|r'\rangle$ state is $\tau_{1/e} = 44(5)$ ns.

2. Simulation details

For the single-photon Rydberg excitations from $^3P_0$, in both the multi-atom Rabi oscillations and single-atom preparation data we observe that the $N = 0$ population increases by more than expected from just the single-atom losses of 0.26(2)%. The population evolutions are consistent with an additional $N \rightarrow N - 2$ loss channel. Thus, we include a two-atom loss modeled with an exponential decay, with phenomenological rate $\tau_{2b}^{(N)}$, which we fit for each $N \geq 2$. From the measured autoionization timescale of 44(5) ns and Rydberg lifetime of 43(2) μs, we estimate a 99.9% probability of autoionizing Rydberg atoms.

APPENDIX D: DETERMINISTIC LOADING

In our experimental results, we do not observe population accumulation at certain atom numbers N (i.e. $N = 4, 9, \ldots$ for $\Delta = 0$), despite operating at a single static detuning. This is a result of ground-Rydberg multi-atom dephasing and two-atom losses. Should these multi-atom Rydberg effects be mitigated in future experiments, the question of optimal pulse sequencing becomes relevant for quick multi-atom removal that prevents population accumulation at certain N. For deterministic loading in the presence of small single and two-atom losses, it is important to control the population evolution so that a majority of the population is successively moved from higher to lower N. One mechanism for controlling the population evolution is to use different detunings at each cycle, in order to engineer higher (or lower) $N \to N-1$ transition rates [see Fig. 6(a)].

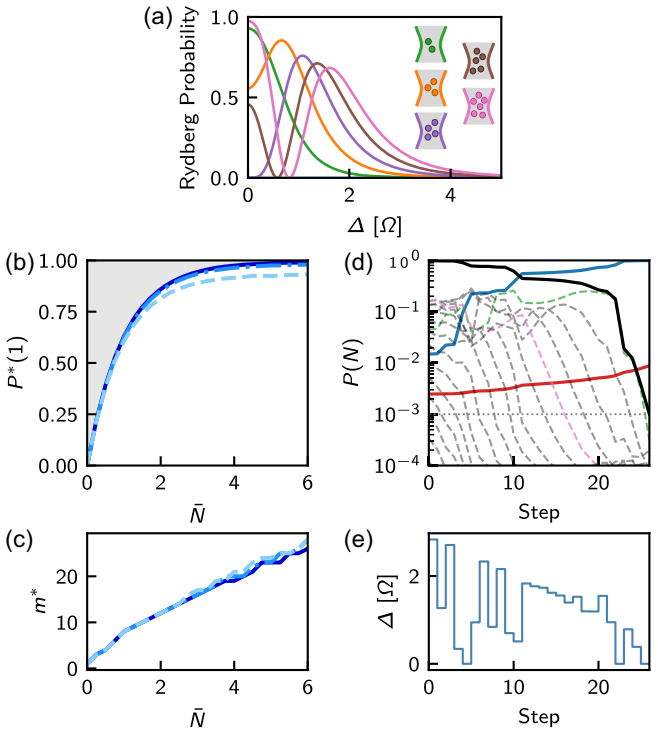


FIG. 6. (a) The probability of exciting a single atom to the Rydberg state for N blockaded atoms as a function of detuning Δ at the single-atom 2π pulse time $T = 2\pi/\sqrt{\Omega^2 + \Delta^2}$, for $N = 2$ through $N = 6$. (b) The single-atom probability, $P^*(1)$, after reaching $P(>1) < 0.1\%$ as a function of $\bar{N}$, for sequences of optimized detunings. The three curves correspond to different single (L_1) and two-atom (L_2) loss probabilities of $\{L_1 = 0.1\%, L_2 = 0.05\%\}$ (solid dark blue), $\{L_1 = 0.25\%, L_2 = 0.25\%\}$ (dot-dashed medium blue), and $\{L_1 = 1\%, L_2 = 1\%\}$ (dashed light blue). (c) The number of cycles required (m^*) to reach $P(>1) < 0.1\%$ as a function of $\bar{N}$, for the sequences corresponding to the curves in (b). (d) The probability evolution for reaching a single-atom filling fraction of 99% with $\bar{N} = 6$ with a single-atom loss probability of 0.1% and two-atom loss probability of 0.05% [dark blue curve in (b,c)]. The solid red, blue, and black lines correspond to $N = 0$, $N = 1$, and $N > 1$. The dashed curves depict $P(N)$ values for individual $N > 1$, with the green and pink curves for $N = 2$ and $N = 6$, respectively, highlighted. (e) The sequence of detunings used at each step to produce the population evolution in (d).

Therefore, we simulate protocols with different detunings for each pulse, based on analytic expressions for superatom Rabi oscillations with small single and two-atom losses. The single-atom losses are modeled based on the Rydberg lifetime, and two-atom losses are modeled as proportional to the pulse length. Given some initial mean number of atoms loaded, $\bar{N}$, and single and two-atom loss probabilities, we find an optimal sequence of detunings $S = \{\Delta_1, \ldots, \Delta_m\}$ by minimizing a cost function

$$C(S) = -P(1)_S + k_1 m + k_2 \theta(P(>1)_S - P_{\text{th}}), \quad \text{(D1)}$$

where $P(1)_S$ and $P(>1)_S$ are the single and multi-atom probabilities after m pulses, P_{th} is a multi-atom threshold, and θ is the Heaviside step function. The constants $k_1 = 0.001$ and $k_2 = 10^3$ penalize longer sequences and sequences that do not yield a multi-atom probability below the threshold, respectively. The first term $-P(1)_S$ maximizes the final single-atom probability. Because $k_1 = 0.001$, a sequence that requires an extra pulse compared to another sequence is only deemed more optimal if it increases $P(1)$ by more than 0.1%.

In Figs. 6(b) and 6(c), we present $P^*(1)$ and m^* as a function of $\bar{N}$, for different single and two-atom loss probabilities. These loss probabilities are given for on-resonant pulses. A single-atom filling fraction of 99% can be reached with a single-atom loss probability of $L_1 = 0.1\%$, two-atom loss probability of $L_2 = 0.05\%$, $\bar{N} = 6$, and $m = 26$. The population evolution and detuning sequence for reaching 99% are shown in Figs. 6(d) and 6(e). Meanwhile, 99.9% can be reached with $L_1 = 0.008\%, L_2 = 0.005\%, \bar{N} = 10$, and $m = 39$.

[1] D. Bluvstein *et al.*, *Logical quantum processor based on reconfigurable atom arrays*, Nature (London) **626**, 58 (2024).

[2] B. W. Reichardt *et al.*, *Fault-tolerant quantum computation with a neutral atom processor*, arXiv:2411.11822.

[3] W. C. Chung *et al.*, *Fault-tolerant operation and materials science with neutral atom logical qubits*, npj Quantum Inf. **11**, 193 (2025).

[4] B. Zhang, G. Liu, G. Bornet, S. P. Horvath, P. Peng, S. Ma, S. Huang, S. Puri, and J. D. Thompson, *Leveraging erasure errors in logical qubits with metastable* ^{171}Yb *atoms*, Nat. Phys. **22**, 910 (2026).

[5] P. Mathiot *et al.*, *Benchmarking a machine-learning differential equations solver on a neutral-atom logical processor*, arXiv:2605.21276.

[6] H. Labuhn, D. Barredo, S. Ravets, S. de Léséleuc, T. Macrì, T. Lahaye, and A. Browaeys, *Tunable two-dimensional arrays of single Rydberg atoms for realizing quantum Ising models*, Nature (London) **534**, 667 (2016).

[7] H. Bernien, S. Schwartz, A. Keesling, H. Levine, A. Omran, H. Pichler, S. Choi, A. S. Zibrov, M. Endres, M. Greiner, V. Vuletić, and M. D. Lukin, *Probing many-body dynamics on a 51-atom quantum simulator*, Nature (London) **551**, 579 (2017).

[8] A. Browaeys and T. Lahaye, *Many-body physics with individually controlled Rydberg atoms*, Nat. Phys. **16**, 132 (2020).

[9] S. Ebadi, T. T. Wang, H. Levine, A. Keesling, G. Semeghini, A. Omran, D. Bluvstein, R. Samajdar, H. Pichler, W. W. Ho, S. Choi, S. Sachdev, M. Greiner, V. Vuletić, and M. D. Lukin, *Quantum phases of matter on a 256-atom programmable quantum simulator*, Nature (London) **595**, 227 (2021).

[10] P. Scholl, M. Schuler, H. J. Williams, A. A. Eberharter, D. Barredo, K.-N. Schymik, V. Lienhard, L.-P. Henry, T. C. Lang, T. Lahaye, A. M. Läuchli, and A. Browaeys, *Quantum simulation of 2D antiferromagnets with hundreds of Rydberg atoms*, Nature (London) **595**, 233 (2021).

[11] J. Choi, A. L. Shaw, I. S. Madjarov, X. Xie, R. Finkelstein, J. P. Covey, J. S. Cotler, D. K. Mark, H.-Y. Huang, A. Kale, H. Pichler, F. G. S. L. Brandão, S. Choi, and M. Endres, *Preparing random states and benchmarking with many-body quantum chaos*, Nature (London) **613**, 468 (2023).

[12] A. Cao, W. J. Eckner, T. Lukin Yelin, A. W. Young, S. Jandura, L. Yan, K. Kim, G. Pupillo, J. Ye, N. Darkwah Oppong, and A. M. Kaufman, *Multi-qubit gates and Schrödinger cat states in an optical clock*, Nature (London) **634**, 315 (2024).

[13] A. L. Shaw, R. Finkelstein, R. B.-S. Tsai, P. Scholl, T. H. Yoon, J. Choi, and M. Endres, *Multi-ensemble metrology by programming local rotations with atom movements*, Nat. Phys. **20**, 195 (2024).

[14] N. Schlosser, G. Reymond, I. Protsenko, and P. Grangier, *Sub-Poissonian loading of single atoms in a microscopic dipole trap*, Nature (London) **411**, 1024 (2001).

[15] N. Schlosser, G. Reymond, and P. Grangier, *Collisional blockade in microscopic optical dipole traps*, Phys. Rev. Lett. **89**, 023005 (2002).

[16] D. Barredo, S. de Léséleuc, V. Lienhard, T. Lahaye, and A. Browaeys, *An atom-by-atom assembler of defect-free arbitrary two-dimensional atomic arrays*, Science **354**, 1021 (2016).

[17] M. Endres, H. Bernien, A. Keesling, H. Levine, E. R. Anschuetz, A. Krajenbrink, C. Senko, V. Vuletic, M. Greiner, and M. D. Lukin, *Atom-by-atom assembly of defect-free one-dimensional cold atom arrays*, Science **354**, 1024 (2016).

[18] H. Kim, W. Lee, H.-G. Lee, H. Jo, Y. Song, and J. Ahn, *In situ single-atom array synthesis using dynamic holographic optical tweezers*, Nat. Commun. **7**, 13317 (2016).

[19] L. Pause, T. Preuschoff, D. Schäffner, M. Schlosser, and G. Birkl, *Reservoir-based deterministic loading of single-atom tweezer arrays*, Phys. Rev. Res. **5**, L032009 (2023).

[20] M. A. Norcia *et al.*, *Iterative assembly of* ^{171}Yb *atom arrays with cavity-enhanced optical lattices*, PRX Quantum **5**, 030316 (2024).

[21] F. Gyger, M. Ammenwerth, R. Tao, H. Timme, S. Snigirev, I. Bloch, and J. Zeiher, *Continuous operation of large-scale atom arrays in optical lattices*, Phys. Rev. Res. **6**, 033104 (2024).

[22] J. A. Muniz *et al.*, *Repeated ancilla reuse for logical computation on a neutral atom quantum computer*, Phys. Rev. X **15**, 041040 (2025).

[23] Y. Li, Y. Bao, M. Peper, C. Li, and J. D. Thompson, *Fast, continuous, and coherent atom reloading in a neutral-atom qubit array*, Science **393**, 1213 (2026).

[24] N.-C. Chiu, E. C. Trapp, J. Guo, M. H. Abobeih, L. M. Stewart, S. Hollerith, P. L. Stroganov, M. Kalinowski, A. A. Geim, S. J. Evered, S. H. Li, X. Lyu, L. M. Peters, D. Bluvstein, T. T. Wang, M. Greiner, V. Vuletić, and M. D. Lukin, *Continuous operation of a coherent 3,000-qubit system*, Nature (London) **646**, 1075 (2025).

[25] J. W. Lis, A. Senoo, W. F. McGrew, F. Rönchen, A. Jenkins, and A. M. Kaufman, *Midcircuit operations using the omg architecture in neutral atom arrays*, Phys. Rev. X **13**, 041035 (2023).

[26] A. Muzi Falconi, R. Panza, S. Sbernardori, R. Forti, R. Klemt, O. Abdel Karim, M. Marinelli, and F. Scazza, *Microsecond-scale high-survival and number-resolved detection of Ytterbium atom arrays*, Phys. Rev. Lett. **135**, 203402 (2025).

[27] A. L. Shaw, A. Soper, D. Shadmany, A. Kumar, L. Palm, D.-Y. Koh, V. Kaxiras, L. Taneja, M. Jaffe, D. I. Schuster, and J. Simon, *A cavity-array microscope for parallel single-atom interfacing*, Nature (London) **650**, 320 (2026).

[28] S. Ma, G. Liu, P. Peng, B. Zhang, S. Jandura, J. Claes, A. P. Burgers, G. Pupillo, S. Puri, and J. D. Thompson, *High-fidelity gates and mid-circuit erasure conversion in an atomic qubit*, Nature (London) **622**, 279 (2023).

[29] P. Scholl, A. L. Shaw, R. B.-S. Tsai, R. Finkelstein, J. Choi, and M. Endres, *Erasure conversion in a high-fidelity Rydberg quantum simulator*, Nature (London) **622**, 273 (2023).

[30] R. Lin, H.-S. Zhong, Y. Li, Z.-R. Zhao, L.-T. Zheng, T.-R. Hu, H.-M. Wu, Z. Wu, W.-J. Ma, Y. Gao, Y.-K. Zhu, Z.-F. Su, W.-L. Ouyang, Y.-C. Zhang, J. Rui, M.-C. Chen, C.-Y. Lu, and J.-W. Pan, *AI-enabled parallel assembly of thousands of defect-free neutral atom arrays*, Phys. Rev. Lett. **135**, 060602 (2025).

[31] S. Wang, W. Zhang, T. Zhang, S. Mei, Y. Wang, J. Hu, and W. Chen, *Accelerating the assembly of defect-free atomic arrays with maximum parallelisms*, Phys. Rev. Appl. **19**, 054032 (2023).

[32] W. Tian, W. J. Wee, A. Qu, B. J. M. Lim, P. R. Datla, V. P. W. Koh, and H. Loh, *Parallel assembly of arbitrary defect-free atom arrays with a multitweezer algorithm*, Phys. Rev. Appl. **19**, 034048 (2023).

[33] X. Wei, Z. Li, A. V. Karve, A. L. Shaw, D. I. Schuster, and J. Simon, *A 10 megahertz spatial light modulator*, arXiv:2601.08906.

[34] E. Bytyqi, J. Sinclair, J. Ramette, and V. Vuletić, *Device for MHz-rate rastering of arbitrary 2D optical potentials*, Opt. Lett. **51**, 3729 (2026).

[35] A. Fuhrmanek, R. Bourgain, Y. R. P. Sortais, and A. Browaeys, *Light-assisted collisions between a few cold atoms in a microscopic dipole trap*, Phys. Rev. A **85**, 062708 (2012).
[36] S. K. Pampel, M. Marinelli, M. O. Brown, J. P. D'Incao, and C. A. Regal, *Quantifying light-assisted collisions in optical tweezers across the hyperfine spectrum*, Phys. Rev. Lett. **134**, 013202 (2025).
[37] D. S. Grün, L. B. Giacomelli, A. Tashchilina, R. Donofrio, F. Borchers, T. Bland, M. J. Mark, and F. Ferlaino, *Light-assisted collisions in tweezer-trapped lanthanides*, Phys. Rev. Res. **8**, 023067 (2026).
[38] T. Grünzweig, A. Hilliard, M. McGovern, and M. F. Andersen, *Near-deterministic preparation of a single atom in an optical microtrap*, Nat. Phys. **6**, 951 (2010).
[39] B. J. Lester, N. Luick, A. M. Kaufman, C. M. Reynolds, and C. A. Regal, *Rapid production of uniformly filled arrays of neutral atoms*, Phys. Rev. Lett. **115**, 073003 (2015).
[40] M. O. Brown, T. Thiele, C. Kiehl, T.-W. Hsu, and C. A. Regal, *Gray-molasses optical-tweezer loading: Controlling collisions for scaling atom-array assembly*, Phys. Rev. X **9**, 011057 (2019).
[41] A. Jenkins, J. W. Lis, A. Senoo, W. F. McGrew, and A. M. Kaufman, *Ytterbium nuclear-spin qubits in an optical tweezer array*, Phys. Rev. X **12**, 021027 (2022).
[42] J. Zhu, C. Chen, L. Zhou, X. Xie, C. Jiang, Z. Ding, F. Wu, F. Yang, G. Wang, Q. Gong, P. Zhang, S. Zhang, and P. Peng, *High-efficiency loading of 2,400 Ytterbium atoms in optical tweezer arrays*, Phys. Rev. Lett. **137**, 063201 (2026).
[43] M. T. DePue, C. McCormick, S. L. Winoto, S. Oliver, and D. S. Weiss, *Unity occupation of sites in a 3D optical lattice*, Phys. Rev. Lett. **82**, 2262 (1999).
[44] E. Vetsch, S. T. Dawkins, R. Mitsch, D. Reitz, P. Schneeweiss, and A. Rauschenbeutel, *Nanofiber-based optical trapping of cold neutral atoms*, IEEE J. Sel. Top. Quantum Electron. **18**, 1763 (2012).
[45] M. Saffman and T. G. Walker, *Creating single-atom and single-photon sources from entangled atomic ensembles*, Phys. Rev. A **66**, 065403 (2002).
[46] M. Ebert, A. Gill, M. Gibbons, X. Zhang, M. Saffman, and T. G. Walker, *Atomic Fock state preparation using Rydberg blockade*, Phys. Rev. Lett. **112**, 043602 (2014).
[47] M. Ebert, M. Kwon, T. G. Walker, and M. Saffman, *Coherence and Rydberg blockade of atomic ensemble qubits*, Phys. Rev. Lett. **115**, 093601 (2015).
[48] A. Gaj, A. T. Krupp, J. B. Balewski, R. Löw, S. Hofferberth, and T. Pfau, *From molecular spectra to a density shift in dense Rydberg gases*, Nat. Commun. **5**, 4546 (2014).
[49] A. Derevianko, P. Kómár, T. Topcu, R. M. Kroeze, and M. D. Lukin, *Effects of molecular resonances on Rydberg blockade*, Phys. Rev. A **92**, 063419 (2015).
[50] M. D. Lukin, M. Fleischhauer, R. Cote, L. M. Duan, D. Jaksch, J. I. Cirac, and P. Zoller, *Dipole blockade and quantum information processing in mesoscopic atomic ensembles*, Phys. Rev. Lett. **87**, 037901 (2001).
[51] I. S. Madjarov, J. P. Covey, A. L. Shaw, J. Choi, A. Kale, A. Cooper, H. Pichler, V. Schkolnik, J. R. Williams, and M. Endres, *High-fidelity entanglement and detection of alkaline-earth Rydberg atoms*, Nat. Phys. **16**, 857 (2020).
[52] A. P. Burgers, S. Ma, S. Saskin, J. Wilson, M. A. Alarcón, C. H. Greene, and J. D. Thompson, *Controlling Rydberg excitations using ion-core transitions in alkaline-earth atom-tweezer arrays*, PRX Quantum **3**, 020326 (2022).
[53] A. Cao, T. L. Yelin, W. J. Eckner, N. D. Oppong, and A. M. Kaufman, *Autoionization-enhanced Rydberg dressing by fast contaminant removal*, Phys. Rev. Lett. **134**, 133201 (2025).
[54] T. Legrand, X. Wang, M. Simić, F. Pausewang, W. Alt, E. Uruñuela, M. T. Eiles, and S. Hofferberth, *Revealing electron-Ytterbium interactions through Rydberg molecular spectroscopy*, Phys. Rev. X **16**, 031045 (2026).
[55] S. J. Evered, D. Bluvstein, M. Kalinowski, S. Ebadi, T. Manovitz, H. Zhou, S. H. Li, A. A. Geim, T. T. Wang, N. Maskara, H. Levine, G. Semeghini, M. Greiner, V. Vuletić, and M. D. Lukin, *High-fidelity parallel entangling gates on a neutral-atom quantum computer*, Nature (London) **622**, 268 (2023).
[56] G. Liu, G. Bornet, D. Kurdak, M. Xiao, C. Li, B. Zhang, and J. D. Thompson, *High-fidelity neutral atom gates leveraging low-rank Hessian optimization*, arXiv:2606.05060.
[57] M. Schlagmüller, T. C. Liebisch, F. Engel, K. S. Kleinbach, F. Böttcher, U. Hermann, K. M. Westphal, A. Gaj, R. Löw, S. Hofferberth, T. Pfau, J. Pérez-Ríos, and C. H. Greene, *Ultracold chemical reactions of a single Rydberg atom in a dense gas*, Phys. Rev. X **6**, 031020 (2016).
[58] P. Geppert, M. Althön, D. Fichtner, and H. Ott, *Diffusive-like redistribution in state-changing collisions between Rydberg atoms and ground state atoms*, Nat. Commun. **12**, 3900 (2021).
[59] Y. Song, K. Kim, J. H. Han, S. Oh, and J. Mun, *High performance imaging of* ^{171}Yb *atom in shallow clock-magic tweezer by alternating dual-tone narrowline cooling*, arXiv:2603.27498.
[60] R. M. Potvliege and C. S. Adams, *Photo-ionization in far-off-resonance optical lattices*, New J. Phys. **8**, 163 (2006).
[61] P. Pillet, W. W. Smith, R. Kachru, N. H. Tran, and T. F. Gallagher, *Microwave ionization of* Na *Rydberg levels*, Phys. Rev. Lett. **50**, 1042 (1983).
[62] T. F. Gallagher, L. M. Humphrey, W. E. Cooke, R. M. Hill, and S. A. Edelstein, *Field ionization of highly excited states of sodium*, Phys. Rev. A **16**, 1098 (1977).